The Astrophysical Journal, 630:L81–L84, 2005 September 1

THE RIGIDLY ROTATING MAGNETOSPHERE OF σ ORIONIS E

R. H. D. Townsend,[1] S. P. Owocki,[1] and D. Groote[2]

Received 2005 March 8; accepted 2005 July 18; published 2005 August 12

ABSTRACT

We characterize the observed variability of the magnetic helium-strong star σ Ori E in terms of a recently developed rigidly rotating magnetosphere model. This model predicts the accumulation of circumstellar plasma in two corotating clouds, situated in magnetohydrostatic equilibrium at the intersections between the magnetic and rotational equators. We find that the model can reproduce well the periodic modulations observed in the star's light curve, Hα emission-line profile, and longitudinal field strength, confirming that it furnishes an essentially correct, quantitative description of the star's magnetically controlled circumstellar environment.

Subject headings: circumstellar matter — stars: chemically peculiar — stars: early-type — stars: individual (HD 37479) — stars: magnetic fields — stars: rotation

1. INTRODUCTION

As befits its status as the archetype of the helium-strong stars, characterized by elevated photospheric helium abundances, the B2 Vpe star σ Ori E is the most studied in its class. This is predominantly due to the rich phenomenology of variability manifested by the star, which exhibits modulations in its Hα Balmer emission (Walborn 1974), its helium absorption-line strengths (Pedersen & Thomsen 1977), its photometric indices (Hesser et al. 1976), its UV continuum flux and resonance-line strengths (Smith & Groote 2001), its 6 cm radio emission (Leone & Umana 1993), its linear polarization (Kemp & Herman 1977), and its longitudinal magnetic field strength (Landstreet & Borra 1978)—all varying on the same 1.19 day period identified with the stellar rotation cycle. Based on these extensive observations, an empirical picture has emerged (e.g., Groote & Hunger 1982; Bolton et al. 1987; Shore 1993) of the star as an oblique dipole magnetic rotator, whose field supports two circumstellar clouds situated at the intersections between the magnetic and rotational equators.

Following on from previous attempts at devising a theoretical basis for this picture (see, e.g., Nakajima 1985; Shore & Brown 1990; Bolton 1994; Short & Bolton 1994), Townsend & Owocki (2005, hereafter TO05) have recently presented a new theoretical model for the distribution of circumstellar plasma around stars, like σ Ori E, that are characterized both by strong magnetic fields (such that the magnetic energy density is very much greater than the plasma energy density) and by significant rotation. The model is built on the notion that plasma, flowing along fixed trajectories prescribed by rigid field lines, experiences an effective potential arising from a combination of the stellar gravitational field and the centrifugal force due to corotation. In the vicinity of points where the effective potential undergoes a local minimum, as sampled along a field line, the plasma can settle into a *stable* configuration of magnetohydrostatic equilibrium.

These concepts, originally advanced by Michel & Sturrock (1974) and Nakajima (1985), are augmented in the TO05 treatment with a description of the process filling the wells established by local potential minima. In a manner similar to the magnetically confined wind shock (MCWS) model envisaged by Babel & Montmerle (1997a, 1997b), radiatively driven wind streams from opposing footpoints collide at the top of closed magnetic loops, producing strong shocks. The postshock plasma cools via radiative emission and then either falls back to the star (see, e.g., ud-Doula & Owocki 2002, their Fig. 4) or—if the rotation is sufficient—settles into an effective potential well, where it continues to corotate in the circumstellar environment and accumulate over time.

A strength of this rigidly rotating magnetosphere (RRM) model is its ability to predict quantitatively, via a semianalytical approach, the relative circumstellar plasma distribution for *arbitrary* magnetic field configurations—not just for the simple axisymmetric case of a rotation-axis-aligned dipole, to which magnetohydrodynamic simulations have so far been restricted on grounds of computational tractability. In particular, application of the RRM formalism to an oblique dipole model star leads to a specific prediction (see TO05) of a density distribution that is sharply peaked into two clouds situated at the intersections between the magnetic and rotational equators. Such a distribution coincides with the observationally inferred picture of σ Ori E; thus, it is clear that the RRM model holds promise for understanding both this particular star and related objects.

This letter presents results from a preliminary investigation into whether the RRM model can *simultaneously* reproduce the spectroscopic, photometric, and magnetic variability exhibited by σ Ori E. Section 2 discusses enhancements we have made to the model since the TO05 study; § 3 then confronts the predictions of the model with the observed behavior of the star. We discuss and summarize our findings in § 4.

2. THEORETICAL DEVELOPMENTS

Although the RRM treatment presented by TO05 is quite general, much of their analysis focuses on the specific case of a spherical star having a dipole magnetic field whose origin coincides with the stellar origin. In the present analysis, we relax both of these restrictions. Specifically, we allow the star to assume a centrifugally distorted figure, by defining its surface not as a sphere but as an isosurface of the effective potential function $\Phi(\boldsymbol{r})$ (see TO05, their eq. [11]). This isosurface is set at $\Phi = GM_*/R_p$, where R_p denotes the polar radius of the star, and here and throughout the other symbols have the same meanings as in TO05.

We also allow for the possibility of a decentered dipole field, by introducing a vector $\boldsymbol{a}$ specifying the displacement of the

[1] Bartol Research Institute, University of Delaware, 217 Sharp Lab, Newark, DE 19716; rhdt@bartol.udel.edu, owocki@bartol.udel.edu.

[2] Hamburger Sternwarte, Gojenbergsweg 112, 21029 Hamburg, Germany; dgroote@hs.uni-hamburg.de.

TABLE 1
RRM Model Parameters

Ω (Ω_c)	ε_*	β (deg)	i (deg)	$\boldsymbol{a}$ (R_p)
0.5	10^{-3}	55	75	(−0.041, 0.30, −0.029)

magnetic origin from the stellar origin. Then, the position vector in the stellar reference frame $\boldsymbol{r}$ is related to the magnetic frame position vector $\tilde{\boldsymbol{r}}$ via

$$\boldsymbol{r} = \mathbf{Q}\tilde{\boldsymbol{r}} + \boldsymbol{a}, \quad (1)$$

where the orthogonal matrix $\mathbf{Q}$ specifies a rotation by an angle β (the dipole obliquity) about the Cartesian y-axis. In the TO05 treatment, $\boldsymbol{a}$ was set to zero, allowing simple expressions (their eq. [21]) to be obtained relating the spherical polar coordinates in each reference frame. For nonzero $\boldsymbol{a}$, such expressions do not exist, but the transformation between frames remains well defined.

3. RRM MODEL

3.1. *General Considerations*

In Table 1, we summarize the basic parameters for the RRM model of σ Ori E. The rotation rate $\Omega = 0.5\Omega_c$ is an estimation based on the star's 1.19 day period, while the scale height parameter ε_* (TO05, eq. [38]) has been assigned a value typical of early-type stars. The choices of the obliquity, $\beta = 55°$, and observer inclination, $i = 75°$, have been guided by certain characteristics of the spectroscopic and photometric observations presented below. In particular, the unequal spacing of the light-curve minima of σ Ori E, whereby the secondary eclipse follows the primary by ~0.4 of a rotation phase (see Fig. 1), restricts the possible RRM geometries to those satisfying the approximate relation $\beta + i \approx 130°$. A further indication that $i \gtrsim 75°$ comes from the fact that at lower inclinations, the Hα variations, which take the form of a double S-wave (see Fig. 2), would exhibit a central spike when the two curves intersect but no such spike is observed in the spectroscopy.

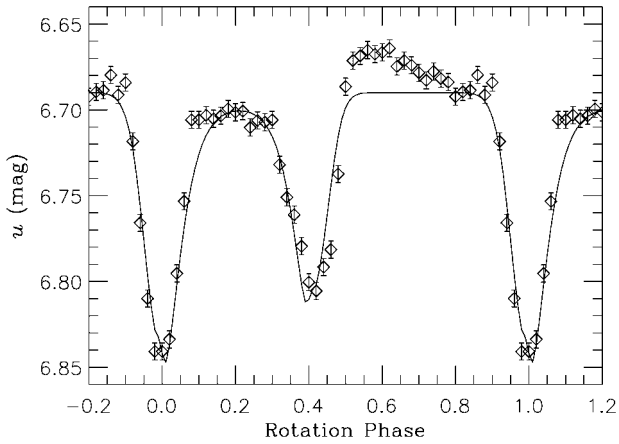

FIG. 1.—Observed (*diamonds*) and modeled (*solid line*) Strömgren *u*-band light curves of σ Ori E, phased on the star's 1.19 day rotation period. The error bars on the observational data are based on conservative estimates of the scatter in the raw data (Hesser et al. 1977, their Fig. 1).

The one remaining parameter of the model is the dipole offset vector $\boldsymbol{a}$. The motivation for assuming a nonzero offset comes from the facts that the primary and secondary eclipses have unequal depths and that the two curves of the double S-wave are of unequal strength. The offset we select comprises (1) a displacement of the dipole center by $0.3R_p$ in a direction perpendicular to both magnetic and rotation axes, followed by (2) a displacement of the dipole center by $-0.05R_p$ along the magnetic axis. The first displacement produces a density contrast between the two clouds situated at the intersections of the equators that allows us to achieve a good fit between the model and the observations. The second displacement has little effect on the circumstellar plasma distribution, but its introduction improves the fit to the magnetic field observations. We note that Short & Bolton (1994) also suggested an offset dipole field in order to explain asymmetries in the field observations.

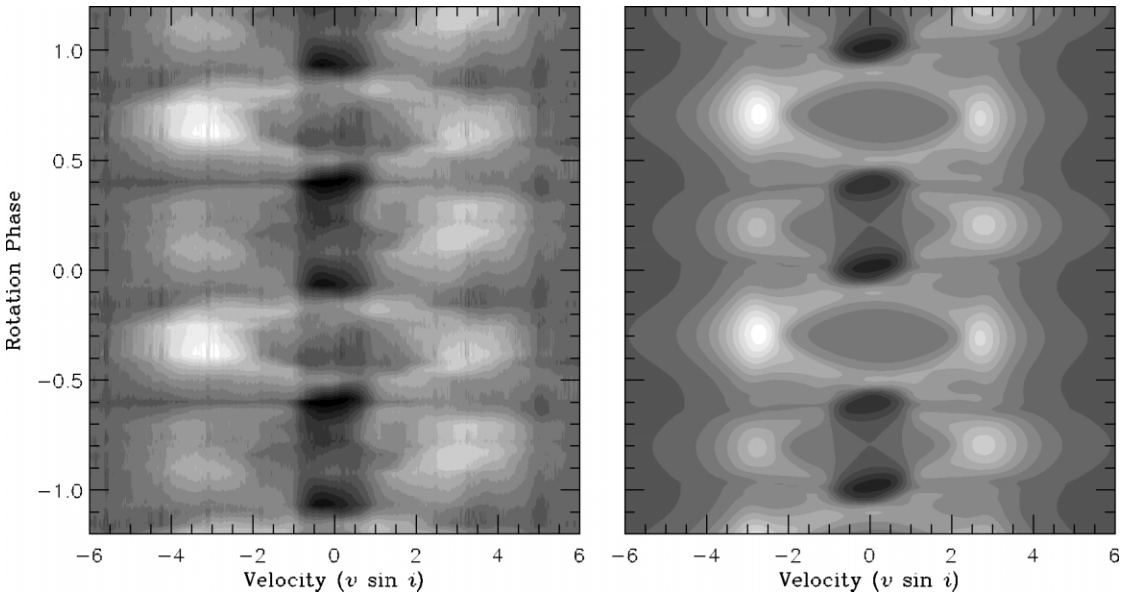

FIG. 2.—Observed (*left*) and modeled (*right*) time-series gray scales of the circumstellar Hα emission of σ Ori E, phased on the star's 1.19 day rotation period. White indicates a 22% excess (in continuum units) over the background photospheric flux, and black indicates a 12% deficit; the gray levels are scaled linearly between these extremes. The velocity axis is expressed in units of the star's projected rotation velocity, $v \sin i = 160$ km s^{-1} (Groote & Hunger 1982).

3.2. *Photometry*

In Figure 1, we show the observed Strömgren *u*-band variations of σ Ori E, obtained via electronic extraction from Figure 2 of Hesser et al. (1977). Over these data we plot the synthetic light curve predicted by the RRM model. To calculate this curve, we assume that the photometric variations arise due to absorption of stellar flux by intervening material confined within the corotating magnetosphere. Then, the observed *u*-band specific intensity I_u, along a given sight line, is evaluated via a simple attenuation expression,

$$I_u = I_* e^{-\tau_u} \tag{2}$$

where I_* is the corresponding intensity at the stellar photosphere and τ_u is the *u*-band optical depth to the photosphere. The variation of I_* across the stellar disk is determined from a combination of the von Zeipel (1924) gravity darkening law (with the *Ansatz* that the intensity varies in proportion to the bolometric flux) and the Eddington (1926) limb darkening law. We calculate τ_u from the density distribution predicted by the RRM model, under the assumption that the opacity in the magnetospheric material is spatially constant; this assumption corresponds, for instance, to bound-free absorption processes in a medium having a uniform composition and excitation state.

Integrating I_u across the stellar disk, we arrive at the synthetic light curve shown in Figure 1. Two free parameters enter into this calculation. The normalization of I_* is chosen so that the intrinsic (unobscured) *u*-band brightness of the star is 6.69 mag. Likewise, the opacity and density are together scaled to achieve a match with the observed depth of the primary eclipse; this scaling corresponds to a maximal optical depth, over all sight lines and rotation phases, of $\tau_u = 1.63$.

The agreement between theory and observations is encouraging; the synthetic light curve manages to capture the timing, duration, and strength of the eclipses. One obvious mismatch is that the RRM model is unable to reproduce the emission feature at phase ~0.6, during which the star appears to brighten above its intrinsic level. However, based on the fact that this feature is conspicuously *absent* from the $u - b$ color variations (see Hesser et al. 1977), we believe the feature may arise from some as yet unknown photospheric inhomogeneity, rather than from the circumstellar material. Further monitoring is required to test this hypothesis.

3.3. *Spectroscopy*

In Figure 2, we plot the circumstellar Hα variations exhibited by σ Ori E, evaluated by subtracting a phase-dependent synthetic absorption profile from spectroscopic observations of the star (25 echelle spectra, obtained during commissioning of the Fiber-fed Extended Range Optical Spectrograph [FEROS] instrument; see Kaufer et al. [1999] and Reiners et al. [2000]). The synthetic profiles are calculated using an updated version of the model atmosphere code of Heber (1983) and a photospheric model (see Groote & Hunger 1997) that takes into account the inhomogeneous helium surface distribution. The resulting synthetic Hδ and Hγ profiles are in very good agreement with the observations, on account of the absence of significant circumstellar contamination in these lines. Assuming that the synthetic Hα profile is also representative of the true (but unknown) photospheric profile, we may interpret the observed minus synthetic difference profiles shown in Figure 2 as an estimated circumstellar component of the total Hα flux.

Alongside the observational data, we plot the corresponding predictions of the RRM model. We calculate the monochromatic specific intensity I_λ at wavelength λ, along a given sight line, via the formal solution to the equation of radiative transfer,

$$I_\lambda = I_* e^{-\tau_\lambda} + S(1 - e^{-\tau_\lambda}); \tag{3}$$

here τ_λ is the monochromatic optical depth, and S is the source function, assumed to be constant and wavelength independent throughout the circumstellar environment. We model the variation of the photospheric intensity across the stellar disk using the same function I_* adopted for the *u*-band synthetic photometry (§ 3.2); since we are ultimately interested only in the circumstellar component of the Hα profile, we do not include any photospheric profile. For sight lines that do not intersect the disk, we set I_* to zero.

To derive the optical depth τ_λ, we assume an opacity proportional to the local plasma density; this choice reflects the fact that Hα absorption and emission, via radiative recombination, are density-squared processes. We further assume that the wavelength dependence of the opacity is a Gaussian of FWHM $\Delta\lambda$, centered on the rest-frame wavelength, 6563 Å, of the line. The modeled spectra are calculated by integrating I_λ across the stellar disk and the surrounding circumstellar region. Three parameters are involved in the synthesis, which we tune by hand to achieve a good fit to the observations. This procedure leads to an intrinsic line width $\Delta\lambda = 30$ km s^{-1}, a source function S set at 0.4 of the maximal photospheric intensity, and an opacity and density scaled such that the maximal optical depth achieved is $\tau_\lambda = 13.4$.

As with the photometry, there is good agreement between theory and observations. The RRM model correctly reproduces all of the qualitative features of the double S-wave Hα variations, including the asymmetry between the red and blue wings, the differing emission strengths at rotation phases ~0.25 and ~0.75, and the absorption features at phases ~0.0 and ~0.4. The phasing of the synthetic data is based on the photometric fit (Fig. 1); thus, the small phase lag of the model, relative to the observations, can wholly be attributed to the uncertainties in the rotation period (see Reiners et al. 2000) compounded over the two decades separating the photometric and spectroscopic data sets. The contrast between the absorption features seen in the observations (strongest at phase ~0.4) and in the model (strongest at phase ~0.0) arises, most likely, due to recent changes in the star's surface abundance distribution (see Groote 2003, his Fig. 3) that are not accounted for in our model.

There are, of course, some discrepancies; for instance, the maximal separation of the S-wave curves is somewhat smaller in the model (~$2.75v \sin i$) than in the observations (~$3.25v \sin i$). Nevertheless, given the many simplifying assumptions incorporated in the RRM model for σ Ori E, it is quite striking how well it matches the observed spectroscopic variability of this star.

3.4. *Magnetic Field*

In Figure 3, we show the time-varying longitudinal magnetic field strength of σ Ori E, as measured by Landstreet & Borra (1978) and Bohlender et al. (1987); to maintain consistency with the spectroscopic data, we rephase the field data using the same period and ephemeris adopted by Reiners et al. (2000). Plotted over the observations is the field strength predicted by the RRM model. These synthetic data are calculated via an approach similar to Stibbs (1950): the longitudinal (observer-directed) field is weighted by the local photospheric intensity I_* introduced previously, integrated across the stellar disk, and

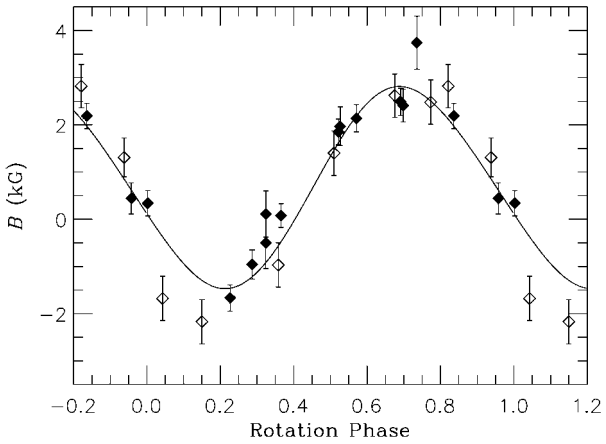

FIG. 3.—Observed (*diamonds*) and modeled (*solid line*) longitudinal magnetic field strength of σ Ori E, phased on the star's 1.19 day rotation period. The open diamonds come from the Landstreet & Borra (1978) data set, while the filled diamonds are taken from the Bohlender et al. (1987) data set.

then renormalized by the disk-integrated flux. The field geometry is specified by the parameters given in Table 1, and we choose a field strength such that the flux density is 11 kG at $\pm 1R_p$ along the magnetic axis. Because the dipole is offset (see § 3.1), the actual surface field strengths at the magnetic poles of the star are somewhat different than this nominal value.

Once again, the agreement between theory and observations is encouraging. The reduced χ^2 of the model, 1.79 for 20 degrees of freedom, is rather larger than the value $\chi^2/n = 1.48$ found by Bohlender et al. (1987) for a sinusoidal fit. However, these authors had the luxury of adjusting the phase of their fit, whereas in the present case the phasing is already constrained by the requirement that the primary light minimum be at phase 0.0 (Fig. 1). We note that if the two outlier points at phases ~0.05 and ~0.15 are discarded, then the correspondence between model and observations improves greatly. Whether these points are indeed erroneous is an matter that should be resolved with further observations.

4. DISCUSSION AND SUMMARY

In §§ 3.2–3.4, we demonstrate how the photometric, spectroscopic, and magnetic variability of σ Ori E can be reproduced extremely well by an RRM model. This is persuasive evidence that the RRM paradigm furnishes an essentially correct, *quantitative* description of the star's magnetically controlled circumstellar environment.

Future studies can now focus on refining the model and its input parameters, beyond the exploratory treatment that we present here. Furthermore, the analysis can be extended to other observable quantities, such as radio emission, UV line strengths, and polarization. Ultimately, based on our coarse exploration of parameter space, we expect that a fully optimized RRM model will be able to provide strong, independent constraints on the fundamental parameters (e.g., mass and radius) of σ Ori E, allowing fresh light to be shed on the historical uncertainty (see Hunger et al. 1989) concerning this exceptional star's distance and evolutionary status.

This work is based in part on support by NASA grant LTSA04-0000-0060 and NSF grant AST 00-97983. We thank the FEROS Consortium and the European Southern Observatory for access to the σ Ori E spectroscopic data.

REFERENCES

Babel, J., & Montmerle, T. 1997a, A&A, 323, 121
———. 1997b, ApJ, 485, L29
Bohlender, D. A., Landstreet, J. D., Brown, D. N., & Thompson, I. B. 1987, ApJ, 323, 325
Bolton, C. T. 1994, Ap&SS, 221, 95
Bolton, C. T., Fullerton, A. W., Bohlender, D., Landstreet, J. D., & Gies, D. R. 1987, in IAU Colloq. 92, Physics of Be Stars, ed. A. Slettebak & T. P. Snow (Cambridge: Cambridge Univ. Press), 82
Eddington, A. S. 1926, The Internal Constitution of the Stars (Cambridge: Cambridge Univ. Press)
Groote, D. 2003, in ASP Conf. Ser. 305, Magnetic Fields in O, B and A Stars: Origin and Connection to Pulsation, Rotation and Mass Loss, ed. L. A. Balona, H. F. Henrichs, & R. Medupe (San Francisco: ASP), 243
Groote, D., & Hunger, K. 1982, A&A, 116, 64
———. 1997, A&A, 319, 250
Heber, U. 1983, A&A, 118, 39
Hesser, J. E., Ugarte, P. P., & Moreno, H. 1977, ApJ, 216, L31
Hesser, J. E., Walborn, N. R., & Ugarte, P. P. 1976, Nature, 262, 116
Hunger, K., Heber, U., & Groote, D. 1989, A&A, 224, 57
Kaufer, A., Stahl, O., Tubbesing, S., Norregaard, P., Avila, G., Francois, P., Pasquini, L., & Pizzella, A. 1999, Messenger, 95, 8
Kemp, J. C., & Herman, L. C. 1977, ApJ, 218, 770
Landstreet, J. D., & Borra, E. F. 1978, ApJ, 224, L5
Leone, F., & Umana, G. 1993, A&A, 268, 667
Michel, F. C., & Sturrock, P. A. 1974, Planet. Space Sci., 22, 1501
Nakajima, R. 1985, Ap&SS, 116, 285
Pedersen, H., & Thomsen, B. 1977, A&AS, 30, 11
Reiners, A., Stahl, O., Wolf, B., Kaufer, A., & Rivinius, T. 2000, A&A, 363, 585
Shore, S. N. 1993, in IAU Colloq. 138, Peculiar versus Normal Phenomena in A-Type and Related Stars, ed. M. M. Dworetsky, F. Castelli, & R. Faraggiana (ASP Conf. Ser. 44; San Francisco: ASP), 528
Shore, S. N., & Brown, D. N. 1990, ApJ, 365, 665
Short, C. I., & Bolton, C. T. 1994, in IAU Symp. 162, Pulsation, Rotation, and Mass Loss in Early-Type Stars, ed. L. A. Balona, H. F. Henrichs, & J. M. Contel (Dordrecht: Kluwer), 171
Smith, M. A., & Groote, D. 2001, A&A, 372, 208
Stibbs, D. W. N. 1950, MNRAS, 110, 395
Townsend, R. H. D., & Owocki, S. P. 2005, MNRAS, 357, 251
ud-Doula, A., & Owocki, S. P. 2002, ApJ, 576, 413
von Zeipel, H. 1924, MNRAS, 84, 665
Walborn, N. R. 1974, ApJ, 191, L95